# Discrete Sliding Mode control of small UAS in tight formation flight under information constraints

**Jan Bolting** * **Soheib Fergani** * **Jean-Marc Biannic** **
**Francois Defay** * **Martin Stolle** **

\* *Institut Supérieur de l'Aéronautique et de l'Espace (ISAE), Toulouse, 31055 France (e-mail: author@ boulder.nist.gov).*
\*\* *Office National d'Études et de Recherches Aérospatiales (ONERA), Toulouse, 31055 Toulouse (e-mail: author@lamar. colostate.edu)*

<span style="color:red">**!!! DRAFT !!!**
Friday 26th February, 2016
14:12</span>

**Abstract:** This paper is concerned with a new control strategy based on discrete sliding mode control of small Unmanned Aerial Systems (UAS) in tight formation flight under information constraints. It addresses the problem of managing and coordinating several UAS to fly in a tight formation. Since the formation of $n$ UAS to be controlled is considered to fly in an arbitrary pattern in this work, a high-performance relative position control becomes an important issue. Indeed, a robust control strategy based on the sliding mode approach is proposed to achieve the desired flight performances while assuming realistic information constraints imposed by limited communication bandwidth and availability of relative localization sensors and preserving scalability with respect to formation size.

Also, this paper presents a meaningful study and comparison of the discrete sliding mode control design (DSMC) and time sampling continuous sliding mode control (TSCSMC). Indeed, it is important to study the performance differences between the two approaches that allow to choose the best strategy to be used to solve the considered problem. Here, the comparison focuses on the effect of the sampling on the control error analytically and in simulation and evaluates effect on mesh stability in simulation.

Simulation results of a flight scenario with two different sampling frequencies proves the efficiency of the proposed control strategy and shows clearly the effect of the discretization and the sampling on the formation flight behaviour of the UAS obtained by the chosen considered control.

*Keywords:* UAS, Formation flight, discrete sliding mode control, robust control.

## 1. INTRODUCTION

The capability of autonomous formation flight has the potential to significantly enhance the utility and efficiency of small low-cost UAS. Formations of small, inexpensive fixed-wing UAS allow for the sharing of remote sensing functionality, mission-level redundancy and range enhancements due to aerodynamic interactions widely exploited by migratory birds. Indeed, aircraft's formation flight can enhance the fuel efficiency thanks to the aerodynamics and the induced airflow by leading aircraft, in the same way that the migratory birds use some formation patterns. Indeed, in Weimerskirch et al. (2001) authors have measured heart rates as an estimate of energy expenditure in imprinted great white pelicans (Pelecanus onocrotalus) trained to fly in 'V' formation, and show that these birds save a significant amount of energy by flying in formation. This advantage is probably a principal reason for the evolution of flight formation in large birds that migrate in groups.

Also, this strategy has a lot of advantages as sharing of remote sensing functionality, mission-level redundancy, range enhancements due to aerodynamic interactions and energy saving. Based on that, the NASA AFF program has demonstrated the feasibility of this approach for manned fighter aircraft in a 2-aircraft configuration. Maximum fuel savings of 14% for the follower are reported. This emphasize on the importance of the flight formation since no structural changes have to be made to the aircraft to gain considerable fuel savings.
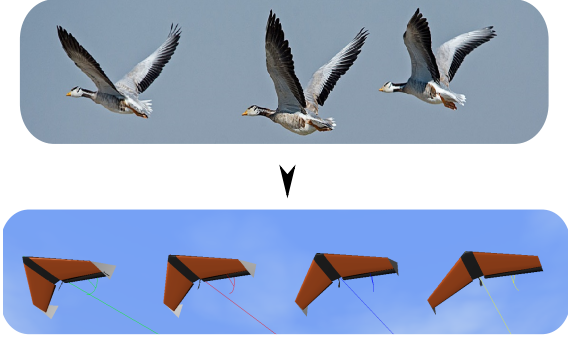
Fig. 1. Formation flight: migrant birds inspiring aircraft performance evolution



Fig. 2. Predecessor-follower geometry longitudinal

## 2. MODEL

### 2.1 Coordinate frames

The system to be controlled is a formation of $n$ UAS flying in an arbitrary pattern. Is is assumed that load factors are controlled in each vehicle's body frame (index $b$). Therefore separation errors are transformed into the body frame for control purposes, decoupling the three axes. The dynamics of each vehicle are defined in a local inertial North-East-Down frame (index $e$).

To dispose of a common reference frame for multiple members of the formation, the **Leader velocity Frame** (index $l$) is defined. Its x axis is aligned with the formation leader's NED speed projected on the horizontal plane, its z axis is aligned with the NED frame's z axis, and its y axis completes a right-handed Cartesian coordinate system. I is used to define the separation vectors that make up the formation.

### 2.2 Vehicle Model

The continuous time vehicle position dynamics w.r.t. the local inertial frame are given by

$$\mathbf{x} = (\mathbf{p} \ \mathbf{v})^T \qquad (1)$$
$$\dot{\mathbf{p}} = \mathbf{v} \qquad (2)$$
$$\dot{\mathbf{v}} = \mathbf{a}_c + \mathbf{a}_w + \mathbf{g} \qquad (3)$$

where $\mathbf{p} \in \mathbb{R}^3$ is the vehicle position, $\mathbf{v} \in \mathbb{R}^3$ is its velocity w.r.t to the local inertial frame, $\mathbf{a}_w \in \mathbb{R}^3$ are accelerations induced by exogenous disturbances such as turbulence and another aircraft's wake, $\mathbf{a}_c \in \mathbb{R}^3$ are commanded accelerations and $\mathbf{g} \in \mathbb{R}^3$ is the gravity vector in the local inertial frame.

It is assumed that load factors $\mathbf{n}_c$ are tracked by fast inner loop controllers in the vehicle body frame, leading to actual load factors $\mathbf{n} = \mathbf{n}_c + \mathbf{n}_w$ where $\mathbf{n}_w = \frac{1}{|\mathbf{g}|}\mathbf{a}_w$ are parasitic load factors introduced by exogenous disturbances and imperfect tracking. This leads to

$$\dot{\mathbf{v}} = \mathbf{R}_{eb}|\mathbf{g}|\mathbf{n}_c + \mathbf{a}_w + \mathbf{g} \qquad (4)$$

Recently, both academical and industrial communities have been very interested in the flight formation of aircrafts and UAS. In Wolfe et al. (1996), decentralized control is presented to increase the efficiency of flight formation of 5 aircraft in a single line. These controllers are derived from a linear model and tested on a linear simulation incorporating a vortex-latting aerodynamics routine. Another interesting study in Thien et al. (2008) focuses on the effect of its position and shape on aerodynamics performances of a given V flight formation. Vortices generated the wing tip of the leader moves downstream forming a pair of opposite rotating line vortices. Some interesting control solutions for autonomous flight formation were introduced in Giulietti et al. (2000). Moreover, in the last decade, a lot of researchers have focused on improving the control strategies to enhance the formation flight performance behaviour. A suitable control strategy for controlling a team of micro-aerial vehicles moving quickly through a three-dimensional environment while maintaining a tight formation is presented in Turpin et al. (2012). Moreover, an interesting control performance analysis for autonomous close formation flight experiments has been achieved in Rice et al. (2014).

In this paper, a discrete robust sliding mode control strategy is proposed to manage the formation flight of UAS. Indeed, sliding mode control has been proved as a very efficient implementable solution for ground vehicle platooning (see Ferrara et al. (2008) and Zou et al. (2013)). Also, the sliding mode control is very efficient and robust approach regarding environmental disturbances to ensure a good position tracking performances. Here, authors provide a robust discrete sliding mode control solution to manage the tight formation flight of the UAS considering external disturbances. Then, a comparison between the discrete time sliding monde control design and the discretization of a time continuous sliding mode control is achieved. Indeed, it proves that the discretization of the time continuous designed controller decreases the tracking performances and the robustness regarding the environmental disturbances. This paper is structured as follows: section...
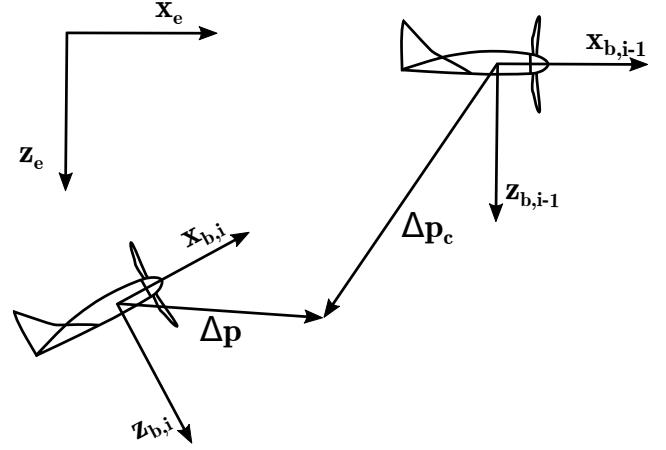
where $\mathbf{R}_{eb} \in \mathbb{R}^{3\times3}$ is the rotation matrix from the body frame to the local inertial frame and $\mathbf{n}_c = \frac{1}{|\mathbf{g}|}\mathbf{a}_c$ are commanded load factors. To simplify notation, is is assumed that the vehicle is trimmed, i.e. the nominal gravitational acceleration is compensated for by a trim control input $\mathbf{n}_{c,0} = \mathbf{R}_{be}(0\ 0\ -1)^T$ and a virtual control input is defined as

$$\mathbf{u} = \mathbf{R}_{eb}|\mathbf{g}|(\mathbf{n}_c - \mathbf{n}_{c,0}) \tag{5}$$

leading to

$$\dot{\mathbf{v}} = \mathbf{R}_{eb}|\mathbf{g}|(\frac{1}{|\mathbf{g}|}(\mathbf{R}_{be}\mathbf{u} + \mathbf{n}_{c,0})) + \mathbf{a}_w + \mathbf{g} \tag{6}$$

$$\dot{\mathbf{v}} = \mathbf{u} + \mathbf{a}_w \tag{7}$$

where now $\mathbf{a}_w$ also includes the small effects of imperfect knowledge of local gravitation. ???doubledefinition

Saturations on the virtual control input (29) can be derived from (17) as

$$|\mathbf{u}| \leq \mathbf{U} \tag{8}$$
$$\mathbf{U} = \mathbf{R}_{eb}|\mathbf{g}|(\mathbf{N} - \mathbf{n}_{c,0}) \tag{9}$$

Considering two UAS $i$ and $i-1$ , this leads to relative position error dynamics

$$\Delta\mathbf{p} = \mathbf{p}_i - \mathbf{p}_{i-1} - \Delta\mathbf{p}_c \tag{10}$$
$$\Delta\dot{\mathbf{p}} = \mathbf{v}_i - \mathbf{v}_{i-1} - \Delta\dot{\mathbf{p}}_c \tag{11}$$
$$\Delta\dot{\mathbf{v}} = \mathbf{a}_i - \mathbf{a}_{i-1} - \Delta\ddot{\mathbf{p}}_c \tag{12}$$
$$= \mathbf{a}_{c,i} + \mathbf{a}_{w,i} - \mathbf{a}_{i-1} - \Delta\ddot{\mathbf{p}}_c \tag{13}$$
$$= \mathbf{u} + \mathbf{a}_{w,i} - \mathbf{a}_{i-1} - \Delta\ddot{\mathbf{p}}_c \tag{14}$$

where $\Delta\mathbf{p}$ is the relative position error between UAS $i$ and its predecessor $i-1$ , $\Delta\mathbf{v}$ is the corresponding relative velocity error, $\Delta\mathbf{p}_c$ is the desired relative position to the predecessor, $\mathbf{a}$ are accelerations.

The presented model is essentially of the same type as that used in Galzi and Shtessel (2006) and provides the benefit of being vehicle-agnostic, as the specific vehicle dynamics are covered by the inner loop load factor controllers. On the other hand, perturbations $\mathbf{a}_w$ and control input saturations are specific to a given vehicle and mission environment. It covers rotary wings as well as fixed wing UAS, which are the focus of this work.

*Formation geometry*   The trajectory of the formation w.r.t. the local inertial frame is defined by the nominal trajectory of a virtual leader aircraft. Arbitrary shapes of the formation can be defined by the relative separation vectors $\Delta\mathbf{p}$.

## 3. CONTROL DESIGN

To benefit from significant aerodynamic performance gains, a follower aircraft needs to stay within a narrow spatial window roughly defined by (see e.g. Jake et al. (2003))

$$-0.2b < \Delta y' < -0.1b \tag{15}$$
$$-0.1b < \Delta z' < 0 \tag{16}$$

while the longitudinal separation $\Delta x'$ is less critical due to slow vortex decay. It is thus the control objective to drive the follower UAS into this window and stay within in.

### 3.1 Input saturations

For a fixed-wing UAS, the maximum load factors are naturally limited by the maximum thrust of the engine and the aerodynamic parameters of the aircraft, such as the stall angle $\alpha_{max}$ as

$$|\mathbf{n}(t)| \leq \mathbf{N}(t) \tag{17}$$

These saturations are time-varying since, including the engine thrust, they are function of the dynamic pressure $\bar{q}(t) = \frac{1}{2}\rho(t)V_a^2(t)$.

### 3.2 Information constraints

It is assumed that observations of the relative position and relative velocity vector between each UAS and its predecessor are available.

This limitation allows to use low-cost vision-based relative localization techniques, which is a significant advantage taking into account the price range of GNSS Real Time Kinematics systems which would be required for localization with respect to the formation leader or other members of the formation that are now within the field of view of onboard vision sensors.

### 3.3 TSCSMC

It is the control objective to drive the system to the sliding surface defined by

$$\sigma(t) = \mathbf{G}\mathbf{x}(t) \tag{18}$$
$$\mathbf{x}(t) = \begin{pmatrix} \Delta\mathbf{p}(t) \\ \Delta\mathbf{v}(t) \end{pmatrix} \tag{19}$$

and, once reached, to keep it on it for all subsequent times $t \geq t^*$. With

$$\mathbf{G} = [\mathbf{G}_1 \mathbf{G}_2] \tag{20}$$

the position error dynamics in sliding mode are

$$0 = [\mathbf{G}_1 \mathbf{G}_2] \begin{pmatrix} \Delta\mathbf{p}(t) \\ \Delta\mathbf{v}(t) \end{pmatrix} \tag{21}$$

$$\Delta\dot{\mathbf{p}} = -\mathbf{G}_2^{-1}\mathbf{G}_1\Delta\mathbf{p} \tag{22}$$

Selecting $-\mathbf{G}_2^{-1}\mathbf{G}_1$ as Hurwitz ensures that $\Delta\mathbf{p}$ asymptotically converges to zero while in sliding mode.

Mesh stability is a feature of a three-dimensional formation of vehicles that allows separation errors to stay locally

contained (see e.g. Pant et al. (2002)). In other words, separation errors between a pair of vehicles are not amplified towards the neighboring vehicle pairs. More vehicles can be added to a mesh stable formation without changing the local controllers, providing scalability. It is a well known fact (Pant et al. (2002)) that linear controllers with local feedback information are mesh unstable.

While in sliding mode, the position error dynamics are by definition confined to (22), independently of adjacent separation errors, implying mesh stability if the system can be kept in sliding mode.

The open loop sliding variable dynamics are

$$\dot{\sigma} = \mathbf{G} \begin{pmatrix} \Delta \mathbf{v} \\ \mathbf{u} + \mathbf{a}_{w,i} - \mathbf{a}_{i-1} - \Delta \ddot{\mathbf{p}}_c \end{pmatrix} \qquad (23)$$

$$= \mathbf{G} \begin{pmatrix} \Delta \mathbf{v} \\ -\Delta \ddot{\mathbf{p}}_c \end{pmatrix} + \mathbf{G} \begin{bmatrix} \mathbf{0} \\ \mathbf{I} \end{bmatrix} (\mathbf{u} + \mathbf{a}_{w,i} + \mathbf{a}_{i-1}) \qquad (24)$$

$$= \mathbf{G}\mathbf{\Phi}_k + \mathbf{G}\mathbf{B}(\mathbf{u} + \mathbf{\Phi}_u) \qquad (25)$$

$$= \mathbf{\Phi}'_k + \mathbf{\Phi}'_u + \mathbf{u}' \qquad (26)$$

The desired relative position $\Delta \mathbf{p}_c$ and its second derivative are communicated to each follower. Accelerations of the predecessor $\mathbf{a}_{k-1}$ as well as exogenous perturbations $\mathbf{a}_w$ acting on the vehicle $i$ are assumed to be unknown but bounded. For notational convenience they are lumped into the disturbance vector $\mathbf{\Phi}_u$

$$\mathbf{\Phi}_u = \mathbf{a}_{w,i} - \mathbf{a}_{i-1} \qquad (27)$$

while the known perturbations $\Delta \ddot{\mathbf{p}}_c$ are redefined as $\mathbf{\Phi}_k$

$$\mathbf{\Phi}_k = \begin{pmatrix} \Delta \mathbf{v} \\ -\Delta \ddot{\mathbf{p}}_c \end{pmatrix} \qquad (28)$$

further defining

$$\mathbf{u}' = \mathbf{G}\mathbf{B}\mathbf{u} \qquad (29)$$

$$\mathbf{\Phi}'_k = \mathbf{G}\mathbf{\Phi}_k \qquad (30)$$

$$\mathbf{\Phi}'_u = \mathbf{G}\mathbf{B}\mathbf{\Phi}_u \qquad (31)$$

Note that all perturbations are assumed to satisfy the matching condition. The three axes are considered decoupled by the inner load factor controllers, allowing for SISO design.

Saturations on the virtual control input (29) can be derived from (17) as

$$|\mathbf{u}'| \leq \mathbf{U}' \qquad (32)$$

$$\mathbf{U}' = \mathbf{G}\mathbf{B}\mathbf{R}_{eb}|\mathbf{g}|(\mathbf{N} - \mathbf{n}_{c,0}) \qquad (33)$$

Since the inner loop load factor controllers cannot track discontinuous reference signals, a continuous control signal is mandatory. The system (25) is of relative degree $\mathbf{r} = (1\ 1\ 1)^T$, thus continuous-time Super-Twisting Sliding Mode controllers (STCSMC, see e.g. Shtessel et al. (2014)) can be applied, providing continuous control signals. We apply the controller presented in Galzi and Shtessel (2006)

extending it trivially from 2D to 3D tracking. The STCSMC controller is then given by

$$u'_p = \alpha_p |\sigma_p|^{1/2}\text{sign}(\sigma_{\mathrm{p}}) + \beta_p \int \text{sign}(\sigma_p)dt \qquad (34)$$

where $p = 1...3$ indicates the three decoupled axes. Adding a term that eliminates the known disturbances $\Phi'_{k,i}$ as in Galzi and Shtessel (2006)

$$u'_p = \alpha_p |\sigma_p|^{1/2}\text{sign}(\sigma_{\mathrm{p}}) + \beta_p \int \text{sign}(\sigma_p)dt - \Phi'_{k,p} \qquad (35)$$

leads to closed loop $\sigma$ dynamics of

$$\dot{\sigma}_p = \alpha_p |\sigma_p|^{1/2}\text{sign}(\sigma_{\mathrm{p}}) + \beta_p \int \text{sign}(\sigma_p)dt + \Phi'_{u,p} \qquad (36)$$

Provided the disturbances $\Phi'_{u,p}$ are bounded by $\Phi'_{u,p} \leq L_p$ controller parameters that fulfill

$$\alpha_p = 1.5\sqrt{L_p} \qquad (37)$$
$$\beta_p = 1.1L_p \qquad (38)$$

drive the system into 2-sliding mode, i.e. $\dot{\sigma} = \sigma = 0$ in finite time. The reaching time is bounded by $t_p^* \leq \frac{7.6\sigma_p(0)}{\beta_p - L_p}$, see Galzi and Shtessel (2006).

The actual control input $\mathbf{n}_c$ is computed from (29, 5) as

$$\mathbf{n}_c = \frac{1}{|\mathbf{g}|}\mathbf{R}_{be}(\mathbf{G}\mathbf{B})^{-1}\mathbf{u}' + \mathbf{n}_{c,0} \qquad (39)$$

using $\mathbf{R}_{eb}^{-1} = \mathbf{R}_{eb}^T = \mathbf{R}_{be}$

*Discretization* For implementation, the STCSMC is sampled with a zero-order hold scheme, leading to the Time-sampled Continuous Sliding Mode controller (TSCSMC). There are results for homogeneous sliding controllers such as the STCSMC (see Shtessel et al. (2014)) stating that the error introduced by discrete sampling is quadratically proportional to the sampling time, i.e. $\sigma = O(T^2)$.

*3.4 DSMC*

Designing a sliding mode controller in the discrete time domain allows to take sampling time effects into account right from the beginning.
The $\sigma$ dynamics assuming forward Euler discretization are

$$\sigma(k+1) = \sigma(k) + T(\mathbf{\Phi}'_k(k) + \mathbf{\Phi}'_u(k) + \mathbf{u}'(k)) \qquad (40)$$

Since a discrete controller has no control over what happens to the continuous system between sampling instants, ideal sliding mode is not achievable. It is however possible to drive the system into so-called quasi-sliding mode, defined by the control objective

$$|\sigma_i(k)| \leq \epsilon_i \qquad (41)$$

for $i = 1...3$, for all $k \geq k^*$ where $\epsilon$ is the width of the quasi-sliding mode boundary layer and $k^*$ is the first sample for which 41 is satisfied, i.e. when the system transitions from the reaching phase into quasi-sliding mode. The proposed DSMC is based on ideas presented by the authors of Monsees and Scherpen (2001) The following simple linear reaching law (proposed e.g. by Spurgeon (1992)) ensures asymptotic convergence to the sliding surface

$$\sigma(k+1) = \boldsymbol{\Psi}\sigma(k) \tag{42}$$

with a diagonal $\boldsymbol{\Psi} \in \mathbb{R}^{3 \times 3}, 0 < \Psi_{i,i} < 1$ for $i = 1...3$. The choice of $\boldsymbol{\Psi}$ allows to trade off control effort and reaching time. Since (42) is equivalent to

$$|\sigma(k+1)| = \boldsymbol{\Psi}|\sigma(k)| \tag{43}$$

the norm of the sliding variable decreases with every time step, indicating convergence to the sliding surface.

*Remark* As mentioned in Monsees and Scherpen (2001), a Lyapunov function does not - as in the continuous case - provide enough constraints to drive the system to the sliding surface without overshoot. This is due to the fact that a Lyapunov function only constrains the direction of the system's motion - towards the sliding surface - but not the magnitude of the next discrete step towards it.

The control input $\mathbf{u}(k)$ required to drive the system (40) according to the reaching law (42) can be computed from the open-loop $\sigma$ dynamics to

$$\mathbf{u}'(k) = \frac{1}{T}(\boldsymbol{\Psi} - \mathbf{I})\sigma(k) - \boldsymbol{\Phi}'_k - \tilde{\boldsymbol{\Phi}}'_u \tag{44}$$

Note that $\mathbf{u}'(k)$ contains an estimate of the unknown perturbations $\tilde{\boldsymbol{\Phi}}'_u(k) = \boldsymbol{\Phi}'_u(k) + \Delta\boldsymbol{\Phi}'_u(k)$. Closing the loop, one obtains

$$\sigma(k+1) = \boldsymbol{\Psi}\sigma(k) + T(\Delta\boldsymbol{\Phi}'_u(k)) \tag{45}$$

Note that the reaching law (42) can not be followed due to the estimation error $\Delta\boldsymbol{\Phi}'_u(k)$. Instead, assuming that initially the system is outside the quasi-sliding mode band, it will approach the sliding surface at least as long as

$$\boldsymbol{\Psi}\sigma(k) \geq T(\Delta\boldsymbol{\Phi}_u(k)) \tag{46}$$

This defines the maximum boundary layer thickness as

$$\epsilon = \boldsymbol{\Psi}^{-1}T(\Delta\boldsymbol{\Phi}_u(k)) \tag{47}$$

A simple way to obtain an estimate of the unknown disturbances is from the previous sample by

$$\boldsymbol{\Phi}_u(k-1) = \sigma(k) - \sigma(k-1) - T(\boldsymbol{\Phi}'_k(k-1) + \mathbf{u}'(k-1)) \tag{48}$$

assuming that the disturbance rate is bounded by $|\frac{d\boldsymbol{\Phi}'}{dt}| \leq \delta\Phi'$, assuming $\boldsymbol{\Phi}'(k) = \boldsymbol{\Phi}'(k-1)$ and a first-order approx-

imation introduces an error $\Delta\boldsymbol{\Phi}'_u(k)$ that is bounded by $|\Delta\boldsymbol{\Phi}'_u(k)| \leq T\delta\Phi'$.

Note that with (47), the boundary layer thickness depends quadratically on the sampling time.

## 4. SIMULATIONS

Both controllers have been evaluated in a simulation environment implemented in Matlab®/Simulink® . In all cases, the closed loop vehicle dynamics have been integrated with a forward Euler scheme. While three-dimensional predecessor tracking is performed, only the vertical channel $\Delta p_3$ is considered here for clarity.

*4.1 Controller parameters*

For the TSCSMC, the controller gains are computed according to (37, 38), requiring the bounds $L_i$ on the maximum unknown perturbations $\Phi'_{u,i}$ which are driven by exogenous disturbances $a_{w,i}$ and acceleration of the predecessor $a_{k-1,i}$.

These being bounded by

$$|a_{w,p}| \leq A_{w,p} \tag{49}$$
$$|a_{i-1,p}| \leq A_{i-1,p} \tag{50}$$

for $i = 1...3$, the bounds on $|a_{w,i}|$ have been obtained empirically from a time series representing 1h of simulated Dryden turbulence at the position of maximum incremental lift in the predecessor's wake filtered by closed loop inner load factor controllers.
The bounds $A_{k-1,i}$ are less obvious, since they depend on the closed-loop behavior of the predecessor. Assuming that the control inputs of the predecessor stay within their saturation limits, i.e.

$$-U_i < \mathbf{u}_{i-1,p} < U_i \tag{51}$$

Now since

$$\mathbf{a}_{i-1} = \mathbf{u}_{i-1} + \mathbf{a}_{w,i-1} \tag{52}$$

$\mathbf{a}_{i-1}$ is bounded by

$$|a_{i-1,p}| \leq U_p + A_{w,p} \tag{53}$$

leading to

$$L_p = U_p + 2A_{w,p} \tag{54}$$

**Remark**: From (54) is becomes clear that no guarantees can be given for the system to stay in sliding mode at all times under the assumption 51. This is due to the fact that the assumption 51 allows the predecessor $i-1$ to apply maximum accelerations that, if at the same time disturbances $\mathbf{a}_{w,p}$ act on the predecessor, cannot be followed by the follower $i$ . Formally this can be checked by computing the equivalent control and its bounds that result from the sliding condition $\dot{\sigma} = \mathbf{0}$ as
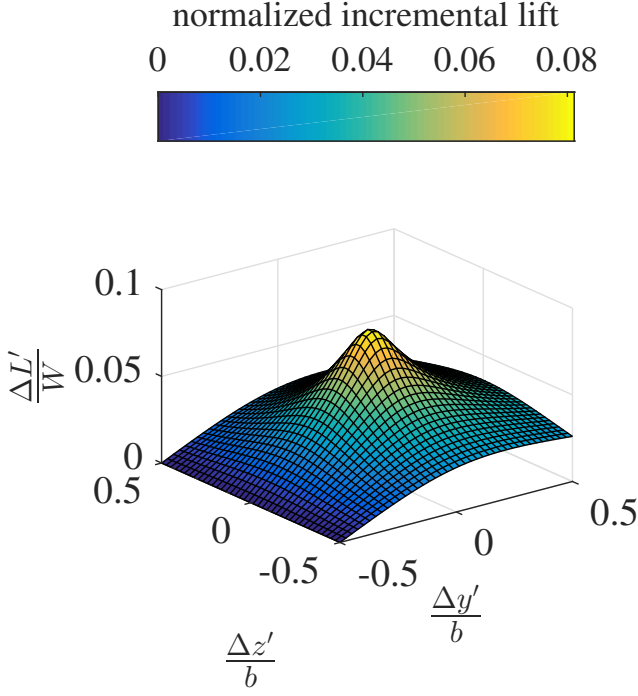
Fig. 3. Normalized incremental lift predicted by modified Horseshoe Vortex Model for $\Delta x' = 2b$. Note that $\Delta x', \Delta y', \Delta z'$ are wingtip to wingtip separations

$$u'_{eq,p} = -\Phi'_{k,p} - \Phi'_{u,p} \tag{55}$$

$$|u'_{eq,p}| \leq \Phi'_{k,p,max} + L_p \tag{56}$$

$$\leq \Phi'_{k,p,max} + U_p + 2A_{w,p} \tag{57}$$

Note that the bounds on $u_{eq,p}$ exceed the control saturations $U_p$.

For the first vehicle pair, which is formed by the virtual leader and the first aircraft, the predecessor control input bounds expressed by (51) can easily be tightened by limiting the second derivative of the virtual leader's trajectory. For the following vehicle pairs, control inputs depend on the sampled closed loop behavior of the controller, which is quite different for the two controllers compared here, as we will see in section 4.

For the DSMC, the entries of the reaching rate matrix $\boldsymbol{\Psi}$ are selected on line to stay within control input limits given the initial error state.

### 4.2 Disturbance models

*Wake vortex disturbances*    A variety of approaches has been proposed to simulate the effects of wake trailing vortices on following UAS, mostly based on modified Horseshoe Vortex Models (HVM) ((!!!citethemall)) or Vortex Lattice methods (VLM) ((!!!citethemall)). For the purpose of this work, a HVM with modified core model presented in (Dogan et al. (2005)) is used. It is reported to provide predictions that are in good agreement of both VLM models and wind tunnel measurements while being of great simplicity. In the vertical channel, the model predicts incremental aerodynamic lift perturbations as a function of the separation vector between a UAS and its predecessor, see fig. 3.
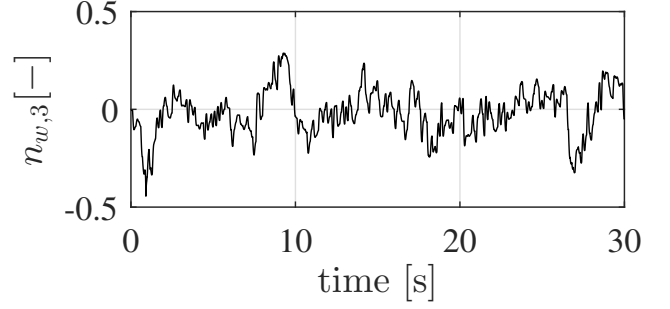


Fig. 4. DSMC controller $10^{-2}s$ sampling time

*Atmospheric turbulence*    Atmospheric turbulence time series are generated according to the Dryden turbulence spectrum. The induced velocities are filtered by transfer functions corresponding to closed loop LQR load factor controllers designed for a small UAS ($b = 2.6m$). An ambient headwind of 20% of the airspeed ($V_a = 15\frac{m}{s}$) is assumed. See fig. 4 for an example time series of the resulting total vertical load factor perturbations $n_{w,3} = \frac{a_{w,3}}{|\mathbf{g}|}$.

*Benchmark maneuver*    To evaluate the control performance, a benchmark maneuver is performed by a formation of 5 UAS. The vehicles start in a staggered formation with relative separations of $\Delta\mathbf{p}_{c,j} = \mathbf{R}_{el}(-2b\ b\ b)^T$ for $j = 1...4$, where $\mathbf{R}_{el}$ denotes the rotation matrix from the leader velocity frame to the local inertial frame. At $t = 5\ s$ the vertical separation is driven to zero, i.e. $\Delta\mathbf{p}_{c,j} = \mathbf{R}_{el}(-2b\ b\ 0)^T$, and each UAS thus enters the zone of maximum incremental lift, see fig. 3. This corresponds to the perturbation $\Delta\ddot{\mathbf{p}}_c$. At $t = 11\ s$ the formation leader performs a climb by $10\ m$, corresponding to the perturbation $\mathbf{a}_{i-1}$.

The benchmark maneuver is run with the TSCSMC controller at $T = 10^{-3}\ s$ and $T = 10^{-2}\ s$. The latter sampling frequency is considered realistic for implementation on board a small UAS. The tracking error $\Delta z = \Delta p_3$ as well the absolute vertical position and the control input is presented in figs. 5, 6. While tracking performance is very good in both cases and the tracking error $\Delta z$ stays well within the bounds indicated by (16), it degrades as expected with lower sampling times. Note that the inputs saturate for large parts of the maneuver, indicating heavy chattering.

The DSMC, on the other hand provides tracking performance at $T = 10^{-2}$ comparable to that of the TSCSMC at $T = 10^{-2}$, see fig. (7). The inputs stay at all times confined to the saturation limits and no chattering is to observed.

This superior performance with respect to lower sampling times is systematically investigated by evaluating the maximum control error and the rms control error over a grid of sampling times, as shown in fig. 8. Note that the rms error and maximum error stays for all sampling times below those of the TSCSMC and evolves more smoothly as the sampling time is varied.
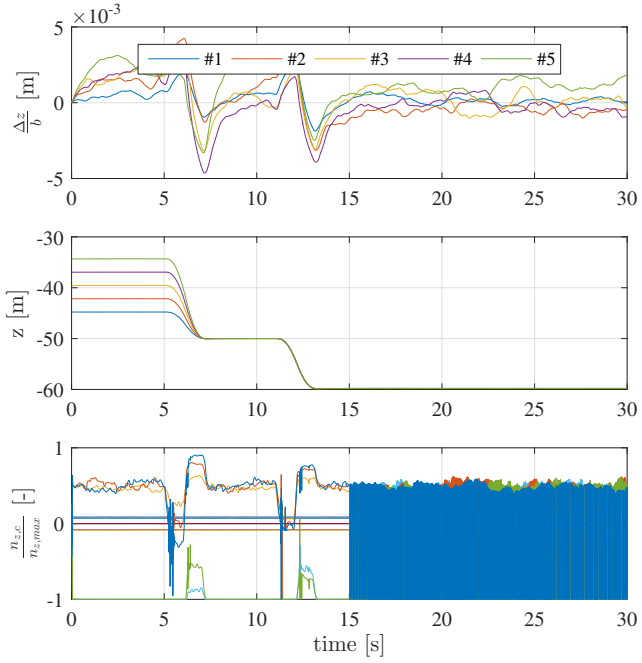
Fig. 5. TSCSMC controller $10^{-3}s$ sampling time
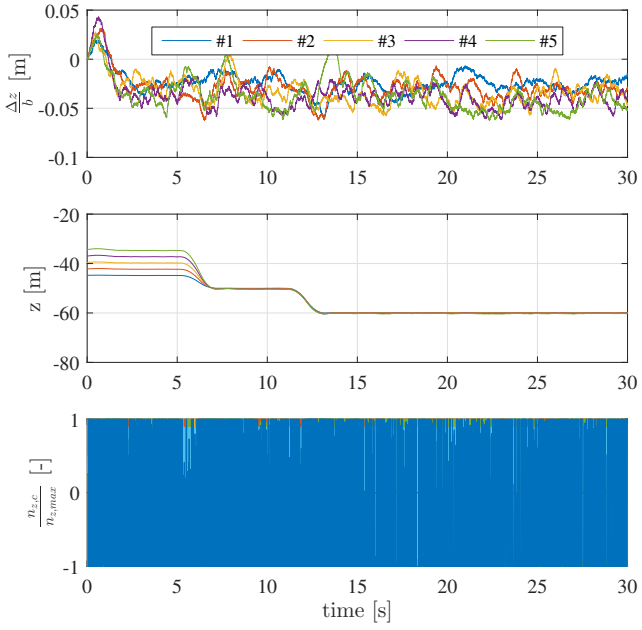


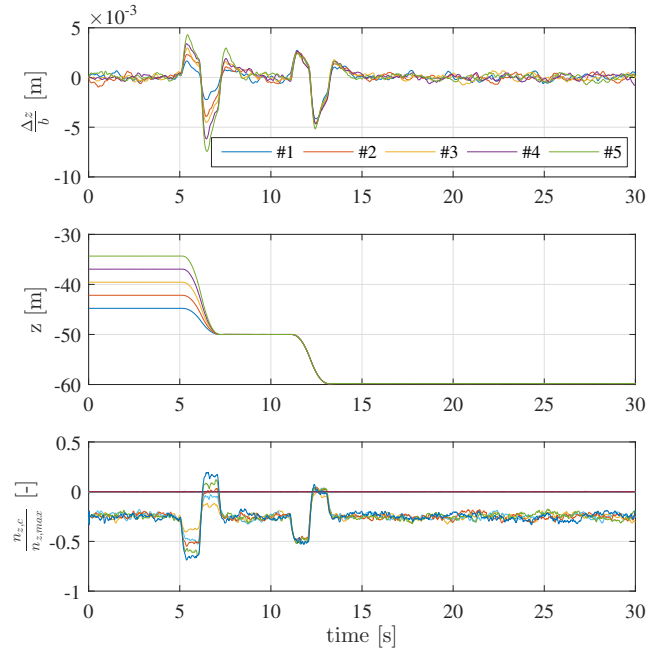Fig. 6. TSCSMC controller $10^{-2}s$ sampling time



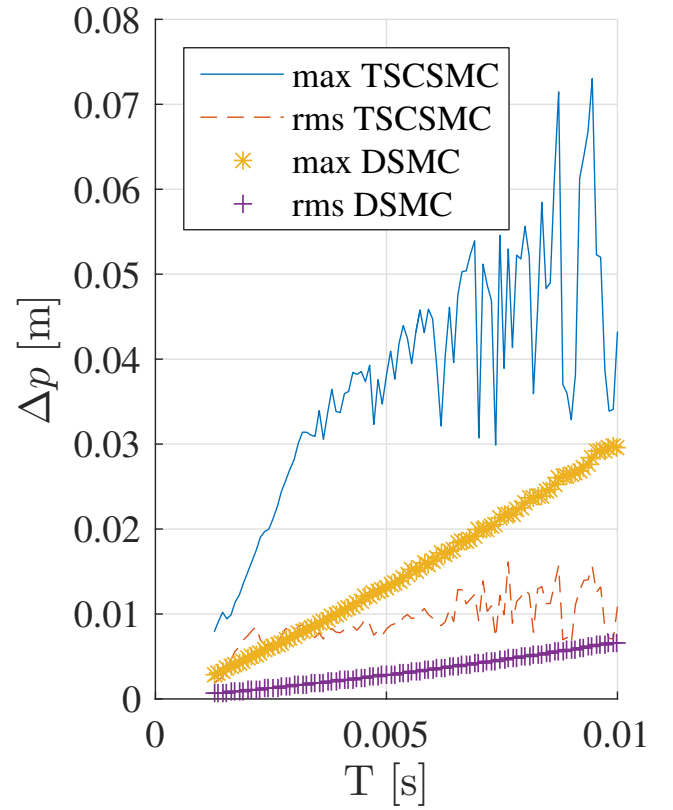Fig. 7. DSMC controller $10^{-2}s$ sampling time



Fig. 8. Vertical position error measures vs. controller sampling time for TSCSMC and DSMC

REFERENCES

Dogan, A., Venkataramanan, S., and Blake, W. (2005). Modeling of aerodynamic coupling between aircraft in close proximity. *Journal of Aircraft*, 42(4), 941–955.

Ferrara, A., Librino, R., Massola, A., Miglietta, M., and Vecchio, C. (2008). Sliding mode control for urban vehicles platooning. In *Intelligent Vehicles Symposium, 2008 IEEE*, 877–882. IEEE.

Galzi, D. and Shtessel, Y. (2006). Uav formations control using high order sliding modes. In *American Control Conference, 2006*, 6–pp. IEEE.

Giulietti, F., Pollini, L., and Innocenti, M. (2000). Autonomous formation flight. *Control Systems, IEEE*, 20(6), 34–44.

Jake, V., Ray, R., Ennix, K., and Walsh, K. (2003). F/a-18 performance beneffts measured during the autonomous formation flight project. Technical report, NASA/TM-2002-210732, Sept.

Monsees, G. and Scherpen, J. (2001). Discrete-time sliding mode control with a disturbance estimator. In *Proceedings of the European Control Conference*, 3270–3275.

Pant, A., Seiler, P., and Hedrick, K. (2002). Mesh stability of look-ahead interconnected systems. *IEEE Transactions on Automatic Control*, 47(2), 403–407.

Rice, C., Gu, Y., Chao, H., Larrabee, T., Gururajan, S., Napolitano, M., Mandal, T., and Rhudy, M. (2014). Control performance analysis for autonomous close formation flight experiments. In *2014 International Conference on Unmanned Aircraft Systems (ICUAS)*.

Shtessel, Y., Edwards, C., Fridman, L., and Levant, A. (2014). *Sliding mode control and observation*. Springer.

Spurgeon, S. (1992). Hyperplane design techniques for discrete-time variable structure control systems. *International Journal of Control*, 55(2), 445–456.

Thien, H., Moelyadi, M., and Muhammad, H. (2008). Effects of leaders position and shape on aerodynamic performances of v flight formation. *arXiv preprint arXiv:0804.3879*.

Turpin, M., Michael, N., and Kumar, V. (2012). Trajectory design and control for aggressive formation flight with quadrotors. *Autonomous Robots*, 33(1-2), 143–156.

Weimerskirch, H., Martin, J., Clerquin, Y., Alexandre, P., and Jiraskova, S. (2001). Energy saving in flight formation. *Nature*, 413(6857), 697–698.

Wolfe, J., Chichka, D., and Speyer, J. (1996). Decentralized controllers for unmanned aerial vehicle formation flight. *AIAA paper*, 96–3833.

Zou, A.M., Kumar, K.D., and Hou, Z.G. (2013). Distributed consensus control for multi-agent systems using terminal sliding mode and chebyshev neural networks. *International Journal of Robust and Nonlinear Control*, 23(3), 334–357.